Using the Quasi-chemical formalism beyond the phase Diagram Density and viscosity models for molten salt fuel systems

Ocádiz Flores, J. A.; Konings, R. J.M.; Smith, A. L.

DOI
10.1016/j.jnucmat.2022.153536

Publication date
2022

Document Version
Final published version

Published in
Journal of Nuclear Materials

Citation (APA)
Ocádiz Flores, J. A., Konings, R. J. M., & Smith, A. L. (2022). Using the Quasi-chemical formalism beyond the phase Diagram: Density and viscosity models for molten salt fuel systems. *Journal of Nuclear Materials*, *561*, Article 153536. https://doi.org/10.1016/j.jnucmat.2022.153536

Journal of Nuclear Materials 561 (2022) 153536

Contents lists available at ScienceDirect

Journal of Nuclear Materials

journal homepage: www.elsevier.com/locate/jnucmat

Using the Quasi-chemical formalism beyond the phase Diagram: Density and viscosity models for molten salt fuel systems

J.A. Ocádiz Flores[a], R.J.M. Konings[a,b], A.L. Smith[a,*]

[a] Faculty of Applied Sciences, Radiation Science & Technology Department, Delft University of Technology, Mekelweg 15, Delft 2629 JB, the Netherlands
[b] European Commission, Joint Research Centre, P.O. Box 2340, Karlsruhe D-76125, Germany

ARTICLE INFO

Article history:
Received 3 August 2021
Revised 11 January 2022
Accepted 12 January 2022
Available online 15 January 2022

Keywords:
Molten Salt Reactor
Quasi-chemical formalism
$NaCl-UCl_3$
$LiF-ThF_4$
$LiF-UF_4$
$LiF-ThF_4-UF_4$

ABSTRACT

CALPHAD models to compute the density and viscosity of four keystone systems related to Molten Salt Reactor (MSR) technology have been optimized: $NaCl-UCl_3$, $LiF-ThF_4$, $LiF-UF_4$, and $LiF-ThF_4-UF_4$. Revised thermodynamic assessments of all four systems, using the modified quasichemical formalism in the quadruplet approximation for the description of the liquid solutions, are reported. In the case of $NaCl-UCl_3$, phase diagram and mixing enthalpy data available in the literature are taken into account. For the fluoride systems, recently published data on some solid phases are taken into account, while retaining the most recently published descriptions of the liquid solutions. The densities of the liquid solutions are modelled using pressure-dependent terms of the excess Gibbs energy, while the viscosities are then modelled using an Eyring equation. Both state functions are related to the thermodynamic assessments through the quadruplet distributions.

1. Introduction

The Molten Salt Reactor (MSR) is a class of fission reactor with the principal characteristic that the fuel is in the liquid state and also serves as the primary coolant [1]. The use of mixtures of uranium tetrafluoride and thorium tetrafluoride with alkali fluorides or beryllium or zirconium fluorides for the fuel system was originally proposed by Ray Briant at the Oak Ridge National Laboratory (ORNL) [2]. Eventually the concept was applied in the construction of the Aircraft Reactor Experiment (ARE) [3], designed, built, and operated by ORNL in the 1950's. Next to these developments, the first conceptual design of a reactor fueled with molten chlorides appears to have been made by Bulmer et al. [4] in 1956. Around the same time, the team at ORNL also considered the use of chloride salts in a fast reactor, as chlorine moderates significantly less than fluorine. However, they pointed out that the high (n,p) cross section of ^{35}Cl, resulting in the formation of corrosive sulphur, would impose the use of ^{37}Cl exclusively. Such an isotope separation is difficult, and so development of fast molten chloride reactors was thought unlikely at the time [2]. Following the ARE, Alvin Weinberg recognized the potential of molten salt reactors as a civilian power source and spearheaded a research program which culminated in the fluoride-fueled, thermal spectrum Molten Salt Reactor Experiment (MSRE), also in ORNL in the 1960's [5]. Despite the great success of the experiment, it was the last prototype MSR to be built. Later, the Generation IV International Forum, a group of fourteen member countries pursuing research and development for the next generation of nuclear reactors, selected the MSR as one of six key nuclear energy systems to replace the current fleet of Generation II Light Water Reactors [6].

Following the historical experience, modern research efforts in the nuclear community have been primarily focused on fluoride salts [7], resulting in a larger (albeit still not fully complete) body of knowledge than for chlorides. Nevertheless, research activities around chloride fuels have increased notably in recent years [8–10]. As pointed out by Merle [11], the design choice depends on the objective. Some advantages of chlorides over fluorides the author has identified are:

1. Lower melting temperatures
2. A wider range of separation processes for salt clean-up, including existing processes
3. Greater actinide solubility
4. Higher breeding ratio when coupled with a U/Pu fuel cycle

While, vice-versa, some of the advantages of the fluorides are:

1. Chemistry is well-characterized for nuclear applications
2. Easier to dehydrate: reduced corrosion risk from initial impurities

* Corresponding author.
E-mail address: a.l.smith@tudelft.nl (A.L. Smith).

https://doi.org/10.1016/j.jnucmat.2022.153536

3. Softer spectrum: reduced radiation damage to structural materials
4. Higher breeding ratio when coupled with a Th/U fuel cycle (epithermal/thermal spectrum)

As for radioisotopes formed during operation, both salt families have problematic products which require careful planning. In a nutshell, the heuristic proposed by Merle is that if the objective is a thorium breeder reactor, a LiF-based salt is more convenient, while for an actinide burner or breeder, NaCl is the main solvent of choice.

This work thus focuses on three keystone binary systems for MSR technology: LiF-UF_4, LiF-ThF_4, and NaCl-UCl_3, as well as the ternary system LiF-ThF_4-UF_4. Two state functions, the density and viscosity are computed. The models are linked to each other via the thermodynamic assessments of the corresponding systems by the CALPHAD method based on the modified quasi-chemical formalism in the quadruplet approximation [12]. The methodology of the density model as applied here was first developed by Robelin et al. [13] on a closely related system sharing NaCl as an end-member, namely NaCl-KCl-$MgCl_2$-$CaCl_2$, and with a well-established industrial application: the reduction of Mg. The same density modelling approach model was later successfully applied to the NaF-AlF_3-CaF_2-Al_2O_3 electrolyte [14]. In further work, Robelin and Chartrand extended the model to compute the viscosity of the same electrolyte [15]. The same methodology is applied herein to our systems of interest, as detailed hereafter.

2. Thermodynamic modelling

2.1. Phase diagrams

A thermodynamic assessment consists of optimizing unknown parameters (e.g. enthalpy of formation, standard entropy) and excess parameters associated with the Gibbs energy functions of all the phases occurring in a system, in order to reproduce known data such as phase diagram equilibria, thermodynamic data, vapor pressure, activities. In this work, FactSage 7.2 was used to perform the thermodynamic assessments.

2.1.1. Pure compounds

The Gibbs energy function of a pure compound is given by:

$$G^o(T) = \Delta_f H^o_m(298) - S^o_m(298)T + \int_{298}^{T} C^o_{p,m}(T)dT - T\int_{298}^{T}\frac{C^o_{p,m}(T)}{T}dT \quad (1)$$

where $\Delta_f H^o_m(298)$ is the standard enthalpy of formation, and $S^o_m(298)$ is the standard absolute entropy, both evaluated at a reference temperature, usually taken to be 298.15 K (throughout this work 298 will be understood to mean 298.15 K for simplicity). $C_{p,m}$ is the isobaric heat capacity expressed as a polynomial:

$$C^o_{p,m}(T) = a + bT + cT^2 + dT^{-2} \quad (2)$$

In the absence of experimental data, the Neumann-Kopp rule [16] was applied to estimate the heat capacities of stoichiometric compounds.

In this work, the thermodynamic functions of the solid phases are very similar to those appearing in the most recent assessments of the systems studied (see Section 2.1.3 below), but slightly adjusted to reflect new experimental data published after the aforementioned assessments. First, the isobaric heat capacities of solid and liquid ThF_4 recently measured by Tosolin et al. [17] were used. The authors also re-calculated the enthalpy of fusion from their corresponding enthalpy increment measurements, and the newly assessed data were selected herein: (36.4 ± 10) kJ· mol^{-1}, while the previous reference value was (41.9 ± 2) kJ· mol^{-1} [18]. The chosen value affects the topology of the LiF-ThF_4 phase diagram (see Fig. 1) but does not affect the quadruplet distributions which serve as input for the viscosity model (see Section 2.3). Second, the heat capacities of $LiThF_5$(cr), $LiTh_2F_9$(cr), and $LiTh_4F_{17}$(cr), measured with Differential Scanning Calorimetry (DSC) by Mukherjee and Dash [19] were taken into account. Third, the LiF-UF_4 system was slightly re-optimized to reflect new insights on the phase equilibria reported in [20]: Li_3UF_7 was included as a metastable phase, and $Li_7U_6F_{31}$ was replaced with $LiUF_5$. These changes required a slight re-optimization of the thermodynamic functions, indicated in bold in Table 1.

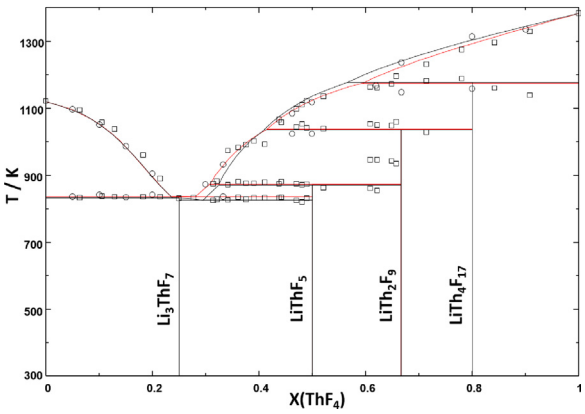

Fig. 1. LiF-ThF_4 diagram as calculated in this work (red), overlaid with the optimization by Capelli et al. [30] (black), and the experimental data reported by Capelli et al. [18] (□) and Thoma et al. [39] (○). (For interpretation of the references to colour in this figure legend, the reader is referred to the web version of this article.)

The thermodynamic functions of NaCl(cr,l) were taken from the IVTAN tables by Glushko et al. [21]. The heat capacity of NaCl(l) was recently recommended by van Oudenaren et al. [22], who critically reviewed the four studies available on the determination of the heat capacity of NaCl(l) [23–26]. Although Glushko et al. had recommended to discard the data by Dawson et al. [26], van Oudenaren et al. [22] found that there was no discrepancy between their data and that reported by the other authors. Averaging over the four studies, van Oudenaren et al. recommend (68 ± 1) kJ·mol^{-1} as the heat capacity of liquid NaCl in the 1074-2500 K range. The heat capacity of UCl_3(l) was also taken from van Oudenaren et al. [22], who derived the value from Molecular Dynamics (MD) simulations. The rest of the thermodynamic functions for UCl_3(cr,l) were taken from the recent review by Capelli and Konings [27].

2.1.2. Solid solution

The total Gibbs energy function of the two-component solid solutions in this work is given by:

$$G(T) = X_1 G^o_{m,1}(T) + X_2 G^o_{m,2}(T) + X_1 RT lnX_1 + X_2 RT lnX_2 + G^{xs}_m \quad (3)$$

where X_i are the molar fractions and $G^o_{m,i}$(T) are the standard molar Gibbs energies of the pure end members. The excess Gibbs energy parameter is described using the polynomial formalism:

$$G^{xs}_m = \sum_{i,j} X_1^i \cdot X_2^j \cdot L_{i,j} \quad (4)$$

where $L_{i,j}$ is a coefficient which may depend on temperature in the form of the general equation:

$$L_{i,j} = A + BT + CTlnT + DT^2 \quad (5)$$

Table 1
Thermodynamic data for end-members and intermediate compounds used in this work for the phase diagram assessment: $\Delta_f H^o_m$(298 K)/(kJ ·mol^{-1}), S^o_m(298 K)/(J·K^{-1}·mol^{-1}), and heat capacity coefficients $C_{p,m}$(T/K)/(J·K^{-1}·mol^{-1}), where $C_{p,m}(T/K) = a + b\cdot T + c\cdot T^2 + d\cdot T^{-2}$. Optimized data are shown in **bold**.

Compound	$\Delta_f H^o_m$(298 K)/ (kJ·mol^{-1})	S^o_m(298 K)/ (J·K^{-1}·mol^{-1})	$C_{p,m}$(T/K)/(J·K^{-1}·mol^{-1})= a + b·T + c·T^2 + d·T^{-2}				Range	Reference
			a	b	c	d		
LiF(cr)	-616.931	35.66	43.309	0.016312	$5.0470\cdot10^{-7}$	$-5.691\cdot10^{5}$	298-2500	[28]
LiF(l)	-598.654	42.962	64.183				298-2500	[28]
ThF_4(cr)	-2097.900	142.05	111.46	$2.6900\cdot10^{-2}$		-780000	298-2500	[29,17]
ThF_4(l)	-2100.360	106.61	168.0				298-2500	[17,29]
UF_4(cr)	-1914.200	151.7	114.5194	$2.0555\cdot10^{-2}$		-413159	298-2500	[29]
UF_4(l)	-1914.658	115.4	174.74				298-2500	[29]
NaCl(cr)	-411.260	72.15	47.72158	0.0057	$1.21466\cdot10^{-5}$	-882.996	298-1074	[21]
			68.0				1074-2500	[22]
NaCl(l)	-383.060	98.407	47.72158	0.0057	$1.21466\cdot10^{-5}$	-882.996	298-1074	[21]
			68.0				1074-2500	[22]
UCl_3(cr)	-863.700	163.9	106.967	-0.02086	$3.639\cdot10^{-5}$	-129900	298-2500	[27]
UCl_3(l)	-846.433	153.6	151.1				298-2500	[27], [22]
Li_3ThF_7(cr)	**-3960.000**	**248.9**	241.387	0.075836	$1.5141\cdot10^{-6}$	$-2.4873\cdot10^{6}$	298-2500	This work
$LiThF_5$(cr)	**-2720.300**	**179.1**	167.8	0.027		$-1.513510\cdot10^{6}$	298-2500	This work, [19]
$LiTh_2F_9$(cr)	**-4820.200**	324.29	291.3	0.0386		$-3.076934\cdot10^{6}$	298-2500	This work, [30,19]
$LiTh_4F_{17}$(cr)	**-9016.100**	609.0	536.2	0.0622		$-5.051854\cdot10^{6}$	298-2500	This work, [30,19]
Li_4UF_8(cr)	**-4347.620**	357.55	287.75532	$8.5804\cdot10^{-2}$	$2.0188\cdot10^{-6}$	-2689653	298-2500	This work, [30]
Li_3UF_7(cr)	**-3777.464**	258.68	244.44634	$6.9491\cdot10^{-2}$	$1.5141\cdot10^{-6}$	-2120530	298-2500	This work
$LiUF_5$(cr)	**-2543.591**	187.4	157.8284	$3.6867\cdot10^{-2}$	$5.0470\cdot10^{-7}$	-982283	298-2500	This work
LiU_4F_{17}(cr)	**-8293.861**	644.7	501.38658	$9.8532\cdot10^{-2}$	$5.0470\cdot10^{-7}$	-2221736	298-2500	This work, [30]

Table 2
Excess Gibbs energy of solid solutions appearing in this study.

Solid solution	ΔG^{xs}_m (J · mol^{-1})	Ref.
(Th,U)F_4	$\Delta\ G^{xs}_m = 400\cdot X_{ThF_4}X_{UF_4}$	[32]
Li_3(Th,U)F_7	$\Delta\ G^{xs}_m = 5500\cdot X_{Li_3ThF_7}X_{Li_3UF_7}$	this work
Li(Th,U)F_5	$\Delta\ G^{xs}_m = -2500\cdot X_{LiThF_5}X_{LiUF_5}$	this work
Li(Th,U)$_2F_9$	$\Delta\ G^{xs}_m = -38000\cdot X_{LiTh_2F_9}X_{LiU_2F_9}$	this work
Li(Th,U)$_4F_{17}$	$\Delta\ G^{xs}_m = -80500\cdot X_{LiTh_4F_{17}}X_{LiU_4F_{17}}$	this work

The values of the excess Gibbs energy parameters of the solid solutions in this study are summarized in Table 2. They belong to the UF_4-ThF_4 and LiF-ThF_4-UF_4 systems. All except the (Th,U)F_4 solution [31] were optimized in this work.

2.1.3. Liquid solution

The excess Gibbs energy terms of liquid solutions herein were modelled using the modified quasi-chemical model in the quadruplet approximation proposed by Pelton et al. [12]. In this formalism, a set of two anions and two cations makes up a quadruplet, taken to be the basic unit in liquid solution, and the excess parameters to be optimized are those related to the following second-nearest neighbor (SNN) exchange reaction:

$$(A-X-A)+(B-X-B)\longrightarrow 2(A-X-B)\quad \Delta g_{AB/X} \tag{6}$$

where the halide anions are represented by X, and A and B denote the cations. $\Delta g_{AB/X}$ denotes the Gibbs energy change associated with the SNN exchange reaction:

$$\Delta g_{AB/X} = \Delta g^0_{AB/X} + \sum_{i\geq 1} g^{i0}_{AB/X}\chi^i_{AB/X} + \sum_{j\geq 1} g^{0j}_{AB/X}\chi^j_{BA/X} \tag{7}$$

$\Delta g^0_{AB/X}$ and $g^{ij}_{AB/X}$ are coefficients which may be taken to be temperature-dependent, but which are independent of composition. The composition dependence is given by the $\chi_{AB/X}$ terms defined as:

$$\chi_{AB/X} = \frac{X_{AA}}{X_{AA}+X_{AB}+X_{BB}} \tag{8}$$

where X_{AA}, X_{BB} and X_{AB} represent cation-cation pair mole fractions. Finally, charge conservation over the quadruplet imposes the anion coordination number:

$$\frac{q_A}{Z^A_{AB/X}} + \frac{q_B}{Z^B_{AB/X}} = \frac{2q_X}{Z^X_{AB/X}} \tag{9}$$

where q_i are the charges of the different ions, and $Z^X_{AB/X}$ is the anion-anion coordination number. For the fluoride systems, the cation-cation coordination numbers, as well as the optimized Gibbs energy terms were taken from previous assessments [30,32] and are shown below for completeness (Table 3, Eqs. (10) and (11)). For NaCl-UCl_3, the Gibbs energy terms were re-optimized in this work to take into account mixing enthalpy data by Matsuura et al. [33] (see Section 3.1.3).

Table 3
Cation-cation coordination numbers of the liquid solutions.

Fluoride solutions [30]			
A	B	$Z^A_{AB/X}$	$Z^B_{AB/X}$
Li^+	Li^+	6	6
Th^{4+}	Th^{4+}	6	6
U^{4+}	U^{4+}	6	6
Li^+	Th^{4+}	2	6
Li^+	U^{4+}	2	6
Th^+	U^{4+}	6	6
Chloride solutions, this work			
Na^+	Na^+	6	6
U^{3+}	U^{3+}	6	6
Na^+	U^{3+}	3	6

$$\Delta g_{LiTh/F} = -10878 + (-6694 + 2.93\cdot T)\chi_{LiTh/F} + (-20920 + 19.25\cdot T)\chi_{ThLi/F}\ J\cdot mol^{-1} \tag{10}$$

$$\Delta g_{LiU/F} = -16108 + (-711.3 - 1.255\cdot T)\chi_{LiU/F} + (-1172 - 8.368\cdot T)\chi_{ULi/F}\ J\cdot mol^{-1} \tag{11}$$

$$\Delta g_{NaU/Cl} = -9865 + 3.5\cdot T - 1150\chi_{NaU/Cl} + (-4100 + 4\cdot T)\chi_{UNa/Cl}\ J\cdot mol^{-1} \tag{12}$$

2.1.4. Higher order systems

The ternary diagram LiF-ThF_4-UF_4 has been extrapolated from the constituting binary sub-systems using the asymmetric Kohler-Toop formalism [34]. The salts belong to two groups of symmetry based on their tendency to remain as dissociated ionic liquid (LiF) or associated species (molecular, network forming) in the melt (ThF_4, UF_4). No ternary excess parameters were used.

2.2. Density model

The density model based on the modified quasi-chemical model was introduced by Robelin et al. [13] and applied to the NaCl-KCl-$MgCl_2$-$CaCl_2$ system, and later to the NaF-AlF_3-CaF_2-Al_2O_3 electrolyte [14].

The volume of a solution is defined as the partial derivative of the Gibbs energy with respect to pressure [13]:

$$V = \left(\frac{\partial G}{\partial p}\right)_{T,n_{A/X},n_{B/X},n_{C/X}} \tag{13}$$

In Eq. (13) the temperature and the number of moles of the constituents are held constant. For a pure halide salt A/X the molar Gibbs energy can be written as:

$$g^o_{A/X}(T,p) = g^o_{A/X}(T,p^o) + \int_{p^o}^{p} V_m^{A/X}(T)\cdot dp = g^o_{A/X}(T,p^o) + V_m^{A/X}(T)\cdot(p-p^o) \tag{14}$$

where p^o is the standard pressure (1 bar) and $V_m^{A/X}(T)$ is the molar volume of the pure salt A/X at temperature T. It is a function of the volumetric thermal expansion $\alpha(T)$:

$$V_m^{A/X}(T) = V_m^{A/X}(T_{ref})\cdot exp\left(\int_{T_{ref}}^{T}\alpha(T)\cdot dT\right) \tag{15}$$

where T_{ref} is an arbitrarily chosen reference temperature and $\alpha(T)$ is given by:

$$\alpha(T) = a + bT + cT^{-1} + dT^{-2} \tag{16}$$

The volume of the solution is then given by:

$$V = \sum_i n_{i/X}\cdot V_m^{i/X}(T) + \sum_A\sum_{A>B}(n_{AB/X}/2)\cdot\left(\frac{\partial \Delta g_{AB/X}}{\partial p}\right)_{T,n_{i/X},n_{A/X},n_{B/X}\ldots} \tag{17}$$

The first term in Eq. (17) represents ideal (additive) volumetric behavior, while the second corresponds to deviations from ideality. $\Delta g_{AB/X}$ can be written as a polynomial in composition parameters (see Eq. (8)) $\chi_{AB/X}$ and $\chi_{BA/X}$:

$$\Delta g_{AB/X} = [\Delta g^o_{AB/X} + \beta^o_{AB/X}\cdot(p-p^o)] + \sum_{i\geq 1}\cdot[g^{i0}_{AB/X} + \beta^{i0}_{AB/X}\cdot(p-p^o)]\cdot(\chi_{AB/X})^i + \sum_{j\geq 1}\cdot[g^{0j}_{AB/X} + \beta^{0j}_{AB/X}\cdot(p-p^o)]\cdot(\chi_{BA/X})^j \tag{18}$$

where p is in bar, and $g^o_{AB/X}$, $g^{i0}_{AB/X}$, and $g^{0j}_{AB/X}$ are parameters from the thermodynamic assessment, while $\beta^o_{AB/X}$, $\beta^{i0}_{AB/X}$, and $\beta^{0j}_{AB/X}$ are the parameters (in general dependent on temperature) which belong to the density model and can be optimized to match deviations from ideality. Note that at 1 bar, the pressure-dependent terms in Eq. (18) cancel out, yet they can still have an effect on the volume through the partial derivative $\left(\frac{\partial \Delta g_{AB/X}}{\partial p}\right)_{T,n_{i/X},n_{A/X},n_{B/X}\ldots}$ (Eq. (17)).

2.3. Viscosity model

Robelin and Chartrand [15] proposed to use the following equation derived by Eyring [35–37] to model the viscosity of molten electrolytes:

$$\eta = \frac{hN_{Av}}{V_m}\cdot exp\left(\frac{G^*}{RT}\right) \tag{19}$$

where h is Planck's constant, N_{Av} is Avogadro's number, V_m is the molar volume, and G^* is the molar activation energy for viscous flow, expressed as a first order polynomial in the quadruplet mole fractions [15], which in turn can be calculated from a thermodynamic model:

$$G^* = \sum_{quad} X_{quad}G^*_{quad} = \sum_{quad} X_{quad}(A_{quad} + B_{quad}\cdot T) \tag{20}$$

such that

$$\eta = \frac{hN_{Av}}{V_m}\cdot exp\left(\frac{\sum_{quad} X_{quad}(A_{quad} + B_{quad}\cdot T)}{RT}\right) \tag{21}$$

Eq. (19) can be re-written as:

$$ln(\eta\cdot V_m) = ln(hN_{Av}) + \sum_{quad} X_{quad}\left(\frac{A_{quad}}{RT}\right) + \sum_{quad} X_{quad}B_{quad}/R \tag{22}$$

leaving A_{quad} and B_{quad} as adjustable parameters for a linear fit of $ln(\eta\cdot V_m)$ vs. $1/T$. In melts with a common anion, G^* (Eq. (20)) reduces to [15]:

$$G^* = \sum_{i,j} X_{ij}G^*_{ij} = \sum_{ij} X_{ij}(A_{ij} + B_{ij}\cdot T) \tag{23}$$

where each i and j are cations and X_{ij} is the mole fraction of $[i-X-j]$ SNN pairs. However, in melts with strong short-range ordering (SRO), a composition dependence may be introduced for the parameter G^*_{ij}, as proposed by Mizani [38], who modelled the viscosity of the NaCl-$MgCl_2$ melt over the entire composition range:

$$G^*_{ij} = (G^*_{ij})^{00} + (G^*_{ij})^{10}\cdot[X_{ii}/(X_{ii}+X_{jj}+X_{ij})] + (G^*_{ij})^{01}\cdot[X_{jj}/(X_{ii}+X_{jj}+X_{ij})] \tag{24}$$

In Eq. (24), each of $(G^*_{ij})^{00}$, $(G^*_{ij})^{10}$, and $(G^*_{ij})^{01}$ are of the form A_{ij} + $B_{ij}\cdot T$. For the halide mixtures in this work, which exhibit strong SRO, it was necessary to use the form proposed by Mizani to obtain adequate fits of the experimental data.

3. Results and discussion

3.1. Thermodynamic assessments

3.1.1. LiF-ThF_4

The optimized phase diagram as calculated with the re-optimized functions for the ternary fluorides (see Section 2.1.1) is shown in Fig. 1 (red). The calculated phase diagram has a slightly better agreement with the liquidus data [18,39] on the ThF_4-rich side than the previous optimization by Capelli et al. [30] from which the excess Gibbs energy parameters of the liquid solution were taken, while there is an overlap of both models on the LiF-rich portion of the phase diagram.

3.1.2. LiF-UF_4

The newly optimized phase diagram is shown in Fig. 2 (red). Once again the parameters of the excess Gibbs energy were taken from Capelli et al. [30] (black lines) for the liquid solution. The agreement between both models is very good, the main difference being the shift from a line compound with formula $Li_7U_6F_{31}$, as was reported by Barton et al. [40] in the first study carried out on this system, to the line compound $LiUF_5$ as shown in more recent studies [20,41].

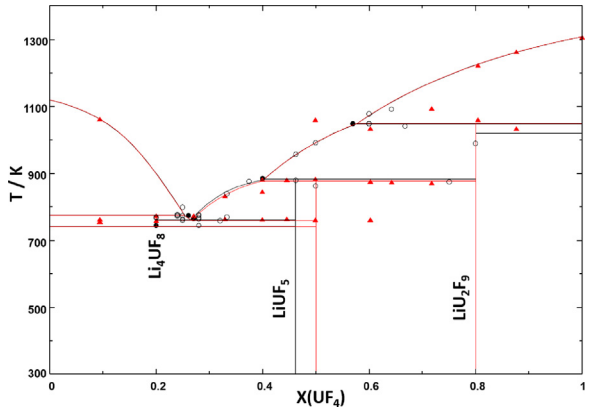

Fig. 2. LiF-UF_4 diagram as calculated in this work (red), overlaid with the optimization by Capelli et al. [30] (black), and the experimental data reported by Ocádiz-Flores et al. [20] (▲) and Barton et al. [40] (○,●). (For interpretation of the references to colour in this figure legend, the reader is referred to the web version of this article.)

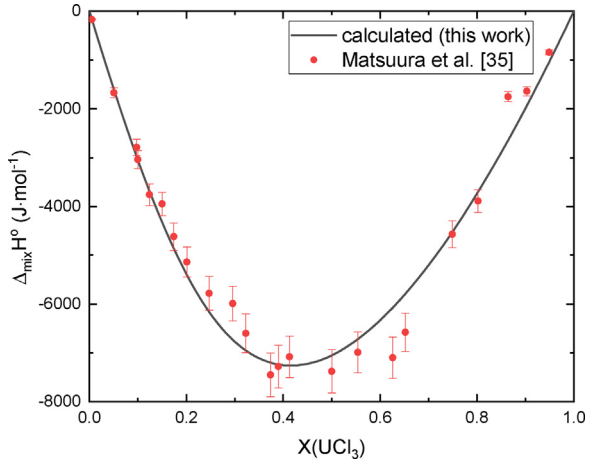

Fig. 3. Calculated enthalpies of mixing in this study (T = 1100 K) for the NaCl-UCl_3 system, compared with the experimental data by Matsuura et al. [33].

3.1.3. NaCl-UCl_3

The choice of $\Delta g_{AB/X}$ (Eq. (7)) which can reproduce a phase diagram with great accuracy, together with the Gibbs energy functions of the rest of the phases in a system, is not unique. Hence, the mixing enthalpy is a very valuable property to assess experimentally as it provides a direct insight into the enthalpic part of the excess Gibbs energy of the liquid solution, and can result in a more physically realistic description. Hence, although a description of NaCl-UCl_3 using the quasi-chemical formalism already exists in the literature [42], it was updated in this study to take into account mixing enthalpy data measured by Matsuura et al. [33] (Fig. 3).

In addition to the mixing enthalpies, equilibrium data by Sooby et al. [43] and Kraus et al. [44] were considered during the optimization process. The calculated phase diagram is shown in Fig. 4. It is a simple eutectic system, with the eutectic point at $X(UCl_3) = 0.33$, $T = (793 \pm 5)$ K according to Kraus, and $X(UCl_3) = (0.34 \pm 0.02)$, $T = (796 \pm 2)$ K according to Sooby et al. [43]. At $X(UCl_3) = 0.35$, $T = 796$ K, the calculated eutectic point in this study closely matches the reported ones.

3.1.4. LiF-ThF_4-UF_4

The ternary LiF-ThF_4-UF_4 phase diagram was experimentally examined by Weaver et al. [45]. In their study, the authors found the UF_4-ThF_4 binary system to be characterized by a solid solution throughout the whole composition range, and four

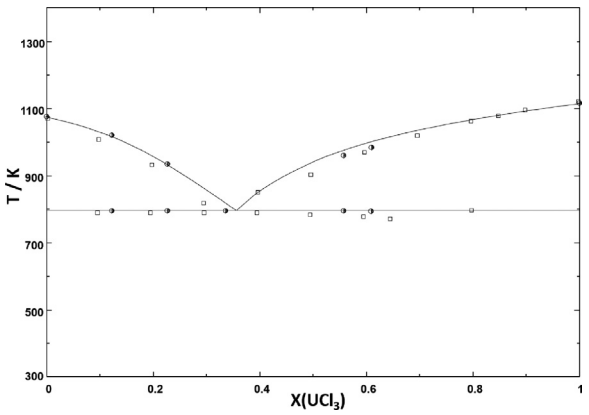

Fig. 4. NaCl-UCl_3 phase diagram as calculated in this work, compared to experimental data by Sooby et al. [43] (◑) and Kraus [44] (□).

solid solutions were reported in the ternary domain: $Li_3(Th,U)F_7$, $Li_7(Th,U)F_{31}$, $Li(Th,U)_2F_9$, and $Li(Th,U)_4F_{17}$. No ternary stoichiometric compounds were observed, and three invariant equilibria were reported (Table 4). Based on these data, thermodynamic assessments were carried out by van der Meer et al. [46], who used a polynomial formalism for the solid and liquid solutions, and later by Beneš et al. [31], who retained a polynomial formalism for the solid solutions but introduced the modified quasi-chemical formalism for the liquid solutions.

From the LiF-ThF_4 (Fig. 1) and LiF-UF_4 (Fig. 2) binary descriptions, the solid solution $Li_7(Th,U)_6F_{31}$ reported by Weaver et al. must in fact correspond to $Li(Th,U)F_5$. As remarked by Beneš et al. [31], the choice of $LiThF_5$ over $Li_7Th_6F_{31}$ does not significantly alter the liquidus line, and the same can be seen in the LiF-UF_4 system (Fig. 2). However, the appearance of solid solutions does significantly alter the liquidus surface over the ternary domain [31], such that it is worthwhile to revise the ternary description with the correct solid solution. In doing so, a liquidus projection congruent with the description by Weaver et al. [45] could be retained, as can be seen in Table 4 and Fig. 5.

3.2. Density and viscosity models for the pure liquid components

The coefficients of the volumetric thermal expansion functions $\alpha(T)$ optimized for the pure liquid salts and their reference molar volume at 298.15 K are given in Table 5. All were derived in this work except those for NaCl, which were taken from Robelin et al. [13]. The molar activation energies for viscous flow, G^*, as optimized in this study, are listed in Table 6.

3.2.1. Density

The density of LiF has been measured by several authors (see Table 7), who report empirical fits of their data. The fit of the thermal expansion coefficient was made based on the empirical equation recommended by Janz et al. [48] in a critical literature review, as the equations reported by most of the other authors reviewed in this work cluster close to it. The calculated density is shown in Fig. 6a, and compared to the empirical equations available in the literature, drawn over the experimentally measured temperature ranges. Apart from the equation by Porter and Meaker [49], which seems to underestimate the density, or that of Brown and Porter [50], which has a markedly different slope, the empirical equations of most authors agree quite well with the empirical equation recommended by Janz et al. [48] (derived by Yaffe and van Artsdalen [51]), and thus with the density calculated in this work (solid line, red, Fig. 6a).

Table 4
Invariant equilibria in the LiF-ThF_4-UF_4 system reported by Weaver et al. [45] and calculated in this study.

X(ThF_4) This study	X(LiF) (calc.)	X(UF_4)	T_{calc} / K	Equilibrium	Solid phases present
0.213	0.641	0.146	899	Peritectic	$Li(Th,U)_2F_9$ + $Li(Th,U)_4F_{17}$ + $Li(Th,U)F_5$
0.087	0.740	0.173	777	Quasi-peritectic	$Li(Th,U)F_5$ + $Li_3(Th,U)F_7$ + LiF
0.019	0.738	0.243	759	Eutectic	$Li(Th,U)F_5$ + LiF + Li_4UF_8
				Weaver et al. [45]	
0.180	0.63	0.19	882	Peritectic	$Li(Th,U)_2F_9$ + $Li(Th,U)_4F_{17}$ + $Li(Th,U)F_5$
0.070	0.725	0.205	773	Peritectic	$Li(Th,U)F_5$ + $Li_3(Th,U)F_7$ + LiF
0.015	0.72	0.265	761	Eutectic	$Li(Th,U)F_5$ + LiF + Li_4UF_8

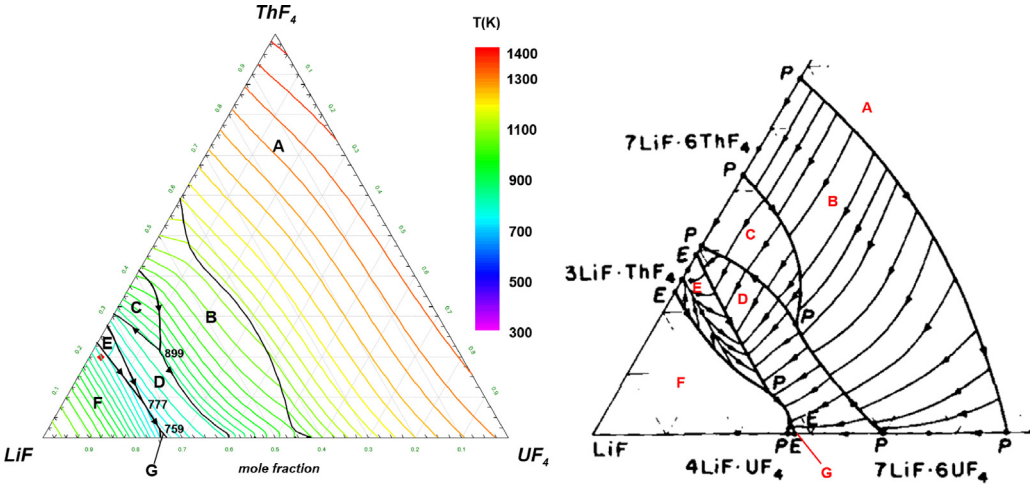

(a) (b)

Fig. 5. (a) Calculated liquidus projection of the LiF-ThF_4-UF_4 system. Invariant equilibria are labelled with the temperatures at which they occur. Isotherms are shown every 25 K. Primary phase fields: (A) $(Th,U)F_4$; (B) $Li(Th,U)_4F_{17}$; (C) $Li(Th,U)_2F_9$; (D) $Li(Th,U)F_5$; (E) $Li_3(Th,U)F_7$; (F) LiF; (G) Li_4UF_8. $Li_{0.775}Th_{0.1995}U_{0.0255}F_{1.675}$ composition studied by Das et al. [47] and modelled in this work (see Section 3.4) is marked as ♦. (b) Detail of the LiF-rich corner of the phase diagram, adapted from Weaver et al. [45], with permission from Wiley and Sons.

Table 5
Molar Volume at 298.15 K and thermal expansion expressions of the pure molten halides.

Liquid salt	V_m^{liquid}(298.15K) / $cm^3 \cdot mol^{-1}$	$\alpha(T)/K^{-1}$			
LiF	12.92	$5.7407 \cdot 10^{-4}$	$-7.9134 \cdot 10^{-8} \cdot T$	$-2.4131 \cdot 10^{-1} \cdot T^{-1}$	$-1.0084 \cdot T^{-2}$
ThF_4	44.66	$9.1509 \cdot 10^{-5}$	$+ 1.9819 \cdot 10^{-8} \cdot T$	$+ 9.5286 \cdot 10^{-1} \cdot T^{-1}$	$-0.9999 \cdot T^{-2}$
UF_4	41.78	$1.0155 \cdot 10^{-4}$	$+ 3.0964 \cdot 10^{-8} \cdot T$	$+ 1.5016 \cdot 10^{-2} \cdot T^{-1}$	$-0.9997 \cdot T^{-2}$
NaCl[a]	29.56	$-0.910 \cdot 10^{-5}$	$+ 2.118 \cdot 10^{-7} \cdot T$	$+ 17.496 \cdot 10^{-2} \cdot T^{-1}$	$-37.278 \cdot T^{-2}$
UCl_3	57.41	$9.8724 \cdot 10^{-5}$	$+ 1.5423 \cdot 10^{-7} \cdot T$	$+ 6.1909 \cdot 10^{-2} \cdot T^{-1}$	$-0.9998 \cdot T^{-2}$

[a] Taken from [13].

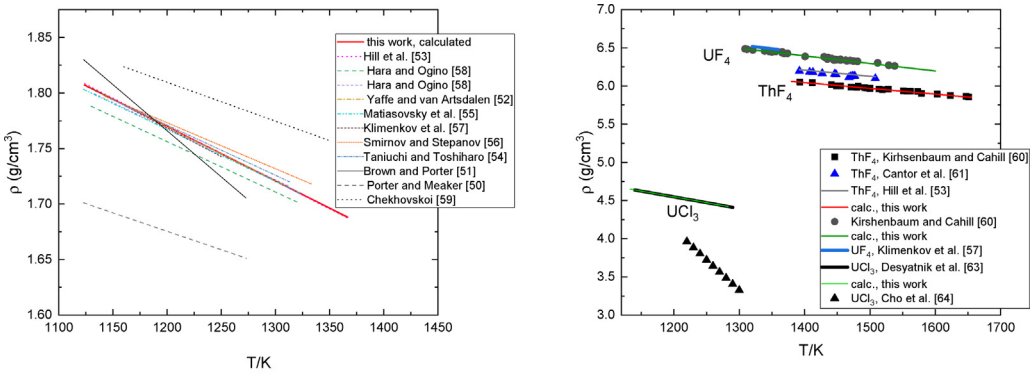

(a) (b)

Fig. 6. Calculated densities of the end-members ((a) LiF, (b) actinide halide end-members) compared to empirical fits (lines) and experimental data (symbols) reported in the literature.

Table 6
Molar viscous activation energy for pure liquid salts.

Liquid salt	$G^* = A + B \cdot T/J \cdot mol^{-1}$	
	A / J · mol^{-1}	B / J · mol^{-1}K^{-1}
LiF	18315.3	18.8078
ThF_4	69033.9	12.1230
UF_4	66145.1	6.7963
NaCl	28296.0	14.1019
UCl_3	21059.2	32.8274

Table 7
Studies of lithium fluoride density.

Reference	Method
Yaffe and van Artsdalen [51]	Archimedean, Submerged bob method
Brown and Porter [50]	Archimedean, quartz spring balance
Porter and Meaker [49]	Archimedean, quartz spring balance
Hill et al. [52]	Archimedean, Pt plummet immersion
Taniuchi and Toshiharo [53]	Archimedean, Pt plummet immersion
Matiasovsky et al. [54]	Archimedean
Smirnov and Stepanov [55]	Maximum bubble pressure, Pt capillary
Klimenkov et al. [56]	Maximum bubble pressure, Ni capillary
Hara and Ogino [57]	Archimedean, Pt plummet immersion
Chekhovskoi [58]	Archimedean, Mo plummet immersion

The density of ThF_4 was first measured by Kirshenbaum and Cahill [59] in 1961, over a rather wide temperature range ranging from 1300 to ~1650 K, using the suspender sinker method (Mo sinkers). A few years later Cantor et al. [60] and Hill et al. [52], both using Pt plummets, made new measurements over a narrower temperature range, which show a density ~2% higher than that reported earlier. Kirshenbaum and Cahill [59] also examined the density of UF_4 over a similar temperature range as ThF_4, and the data were in good agreement with the empirical equation proposed by Klimenkov et al. [56]. Based on the recommendation of van der Meer and Konings [61], the density data selected for these two salts are those by Kirshenbaum and Cahill (Fig. 6b).

Desyatnik et al. (method of maximum bubble pressure) [62] and Cho et al. (pycnometric method) [63] measured the density of UCl_3, with widely differing results (Fig. 6b). Molecular dynamics simulations [64–67] align more closely with the results of the former authors, so their data were taken as the basis for optimization in this work. As will be seen in Section 3.3, this choice also works well when computing the molar volume of the NaCl-UCl_3 binary system.

3.2.2. Viscosity

Several experimentally derived fits describing the viscosity of LiF as a function of temperature are found in the literature [68–72], although only Ejima et al. [73] and Abe et al. [74] explicitly report their experimental points. Both groups used an oscillating vessel viscometer, and their data are in excellent agreement with each other, as is the viscosity computed with the model (Fig. 7). The agreement with the empirical fit derived by Chervinskii et al. [69], who most likely[1] used the rotational oscillation of a liquid-filled cylindrical crucible, is also very good.

Following the recommendation of Janz et al. [48], the viscosity of NaCl was modelled after the empirical fit derived by Murgulescu and Zuca (oscillating sphere method) [76] based on their measurements. The fit derived by Desyatnik et al. (damped rotational oscillations) [62], correlates very well with the reference values. For each of the three actinide halide end-members there is only one study available. Desyatnik et al. [62] studied the viscosity

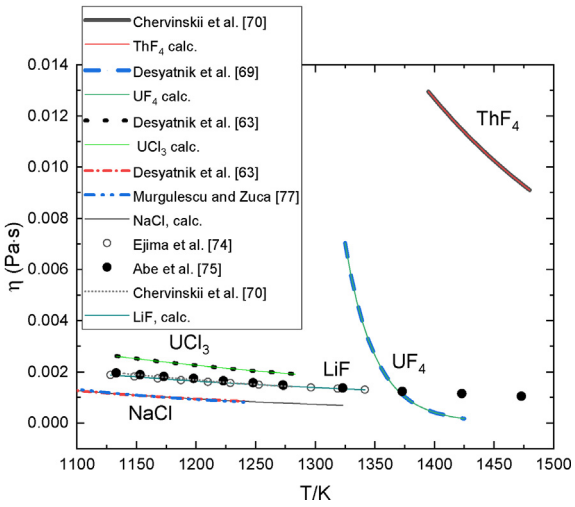

Fig. 7. Calculated viscosities of the pure liquid end-members, compared to empirical fits (solid and dashed lines) and experimental data (●, ○) reported in the literature.

Table 8
Molar viscous activation energy for liquid binary mixtures.

System		G_{ij}^{00}	G_{ij}^{10}	G_{ij}^{01}
LiF-ThF_4	A_{ij}	29011.0	9269.1	-13275.4
	B_{ij}	23.5862	7.5359	-10.8
LiF-UF_4	A_{ij}	24738.7	6254.0	-14161.7
	B_{ij}	20.1127	5.0845	-11.5136
NaCl-UCl_3	A_{ij}	27157.8	-3734.7	
	B_{ij}	22.0795	-3.0363	

A_{ij} in $J \cdot mol^{-1}$, B_{ij} in $J \cdot mol^{-1}K^{-1}$.

of UCl_3 in the range 1128–1278 K. Desyatnik et al. [68] measured the viscosity of UF_4 in the range 1324–1428 K. Both studies used the method of damped rotational oscillations. Finally, Chervinskii et al. [69] measured the viscosity of ThF_4, probably using the same method[2]). The empirical fits to the data in each of the studies could all be modelled successfully (Fig. 7).

3.3. Density and viscosity models for the binary systems

Pressure-dependent contributions to the excess Gibbs energy of mixing (Eq. (6)) needed to be optimized for the NaCl-UCl_3 system only:

$$\Delta g^{p}_{NaU/Cl} = (0.7038 - 0.6819\chi_{NaU/Cl} - 0.3511\chi_{UNa/Cl}) \cdot (p - p^{o}) \ J \cdot mol^{-1} \quad (25)$$

The optimized molar activation energies for viscous flow, G^{*}_{ij} (Eq. (24)), are listed in Table 8.

3.3.1. Density

The densities of LiF-ThF_4 mixtures were measured by Brown and Porter [50] and Porter and Meaker [49] using a quartz spring balance. Hill et al. [52] also performed measurements using a similar method, with a Pt plummet; there is a good correlation between the datasets (Fig. 8a). All authors observed additivity. The ideal behavior of the density can be seen clearly when the molar volumes are plotted: there is a linear dependence with respect to the composition (Fig. 8b). The same holds true in LiF-UF_4 mixtures, which were also measured by Brown and Porter [50], as well

[1] Original work not available to us, but results summarized in [75].

[2] Original work was not available to us, but the results were summarized in [75].

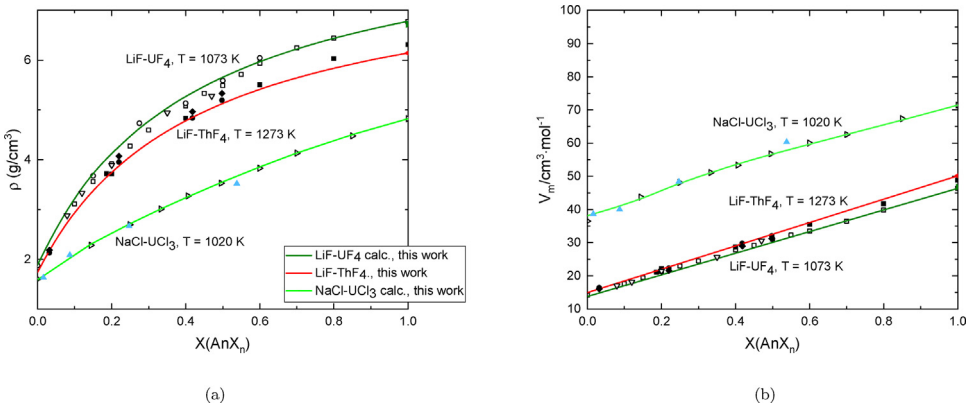

Fig. 8. (a) Calculated densities and (b) molar volumes of the binary mixtures compared to empirical equations and experimental data reported in the literature. LiF-UF_4: Klimenkov et al. [56] □, Brown and Porter [50] ○, Blanke et al. [77] ▽; LiF-ThF_4: Hill et al. [52] ■, Brown and Porter [50] ♦, Porter and Meaker [49] ●; NaCl-UCl_3: Desyatnik et al. [62] ▷, Mochinaga et al. [63] ▲.

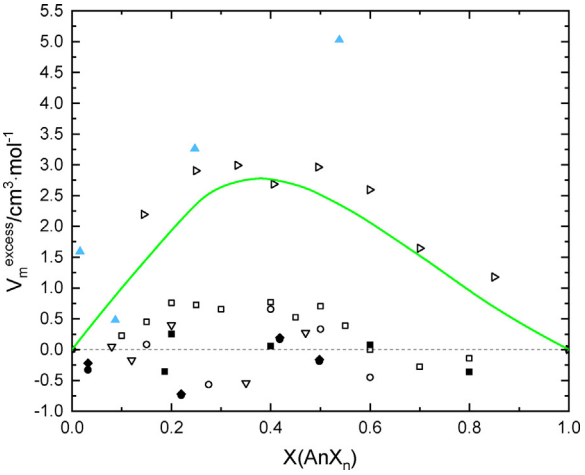

Fig. 9. Excess molar volumes of the binary mixtures: LiF-UF_4 at T =1073 K, LiF-ThF_4 at T = 1273 K, NaCl-UCl_3 at T = 1020 K. Ideal behavior (dotted line), is calculated using the molar volumes of the end-members from the corresponding study, estimated from linear fits when not available. Green solid line: NaCl-UCl_3, this work. LiF-UF_4: Klimenkov et al. [56] □, Brown and Porter [50] ○, Blanke et al. [77] ▽; LiF-ThF_4: Hill et al. [52] ■, Brown and Porter [50] ♦, Porter and Meaker [49] ●; NaCl-UCl_3: Desyatnik et al. [62] ▷, Mochinaga et al. [63] ▲. (For interpretation of the references to colour in this figure legend, the reader is referred to the web version of this article.)

as Blanke et al (Pt plummet) [77]. Klimenkov et al. [56], who used the method of maximum pressure in a gas bubble, found only very slight positive deviations from ideality in this system. Ideal behavior was retained in this work.

Fig. 9 shows the excess molar volumes, calculating the ideal behavior (dotted line) from the volumes of the end-members in the corresponding study (estimated from linear fits when not available). The molar volume of NaCl-UCl_3 mixtures, measured by Mochinaga et al. (pycnometric method) [78] as well as Desyatnik et al. (method of maximum bubble pressure) [62], show a greater deviation from ideality than the tetrafluoride-based melts. This had to be accounted for by introducing pressure-dependent parameters in the excess Gibbs free energy (Eq. (25)). This larger deviation from ideality is probably related to a partial loss of ionic character and increased covalency in the melt [62]. In other words, the formation of molecular ions probably contributes to the free volume. There is spectroscopic evidence of such oligomerisation taking place in LiCl-UCl_3 melts [79], and NaCl-UCl_3 behaves similarly according to MD simulations [64–67]. Incidentally, so do LiF-AnF_4 (An = Th, U) melts [20,75,80,81], yet the smaller volume of Li^+, better suited to occupy interstitial spaces, may explain the difference.

3.3.2. Viscosity

Fig. 10 a shows the isothermal viscosities of the three salt fuel systems at a representative temperature of 1230 K, computed with the model described herein and with the experimentally derived fits found in the literature, with quite a good agreement. All three melts become "polymeric" (there is network formation and short-range ordering) when the actinide halide concentration is high enough [20,64–67,75,80,81], and the increase in viscosity with increasing actinide content is related to a greater extent of formation of associated structures [75]. The tetrafluoride-based melts are more viscous than the trichloride one, as the actinide halide end-members themselves (Fig. 7). This can be attributed to the greater ionic character of the tetrafluoride melts. In molten salts, cations carry anions with them as they diffuse [82–84]. In the tetrafluoride melts, the average An-F distance is ~2.32–2.34 Å for An = Th, and ~2.26–2.28 Å for An= U according to X-ray Absorption spectroscopy (XAS) and MD simulations [85]. In NaCl-UCl_3, MD simulations show and average U-Cl distance of around 2.8 Å [65], in good agreement with X-ray diffraction (XRD) measurements [64]. This suggests fluorides are bound more tightly than the chlorides around the actinide center to which they are coordinated, contributing to a greater viscosity.

Fig. 10a shows the isomolar viscosities as a function of temperature, at compositions close to the eutectics in the different systems: X(ThF_4) = 0.30, X(UF_4) = 0.275, and X(UCl_3) = 0.30. The agreement is better at higher temperatures. NaCl-UCl_3 has the best agreement throughout both the isomolar and isothermal sections, since the viscosities of the end-members are closer to each other.

3.4. Density and viscosity models of the LiF-ThF_4-UF_4 ternary system

Only one composition has been studied for both density and viscosity, corresponding to fresh MSR fuel: $Li_{0.775}Th_{0.1995}U_{0.0255}F_{1.675}$, by Das et al. [47] (Fig. 5a, ♦). The authors studied the density over the 843–943 K temperature range using the Archimedean method with a Pt sinker and wire, while the viscosity was studied over the range 873–931 K using the parallel plate method. The optimized molar activation energies for viscous flow, G^*_{ij} (Eq. 24), are listed in Table 9.

The empirical equation for the molar volume of $Li_{0.775}Th_{0.1995}U_{0.0255}F_{1.675}$ derived by Das et al. is plotted in Fig. 11 (red dotted line). The molar volume falls between that of the pure end-members, although there is a large excess compared to

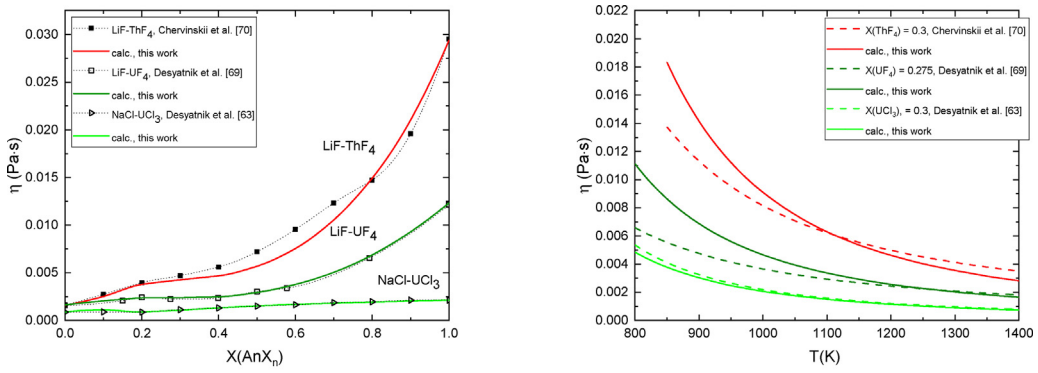

(a) (b)

Fig. 10. (a) Isothermal (T = 1230) viscosities and (b) isomolar viscosities of the binary mixtures computed with the present thermodynamic models and with empirical fits reported in the literature.

Table 9
Molar viscous activation energy for the liquid ternary solution LiF-ThF_4-UF_4.

System		G^{00}_{ThU}	G^{10}_{ThU}	G^{01}_{ThU}
LiF-ThF_4-UF_4	A_{ThU}	-11334638	15800299	
	B_{ThU}	723.267		

A in $J \cdot mol^{-1}$, B in $J \cdot mol^{-1}K^{-1}$.

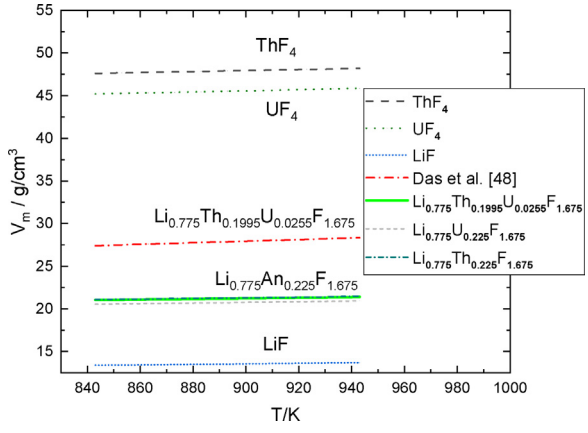

Fig. 11. Molar volume of the $Li_{0.775}Th_{0.1995}U_{0.0255}F_{1.675}$ melt as determined experimentally [47] (red line), compared to the calculated (ideal) behavior, the end-members, and the ideal behavior predicted for the $Li_{0.775}An_{0.225}F_{1.675}$ (An = ThF_4, UF_4) binary mixtures with the present thermodynamic models. (For interpretation of the references to colour in this figure legend, the reader is referred to the web version of this article.)

ideal behavior (light green), itself practically identical to the molar volume of the $Li_{0.775}Th_{0.255}F_{1.675}$ solution, and slightly higher than that of the $Li_{0.775}U_{0.255}F_{1.675}$ solution. Like the LiF-based binaries, ThF_4-UF_4 is expected to form an ideal liquid solution –the phase diagram can be modelled successfully by treating the melt as such [31]. The ternary phase diagram can also be modelled successfully without any excess ternary terms, see Section 2.1.4, and it is difficult to explain why the molar volumes of the ternary mixture should deviate so much, if at all, from ideality. Thus, for the subsequent calculation of the viscosity, an ideal molar volume has been retained. For the viscosity computation, only the G^{00}_{ThU} and G^{10}_{ThU} terms, associated with the Th-U quadruplets, needed to be optimized, with good results (Fig. 12). More compositions, preferably richer in UF_4, would need to be measured to evaluate the robustness of this model.

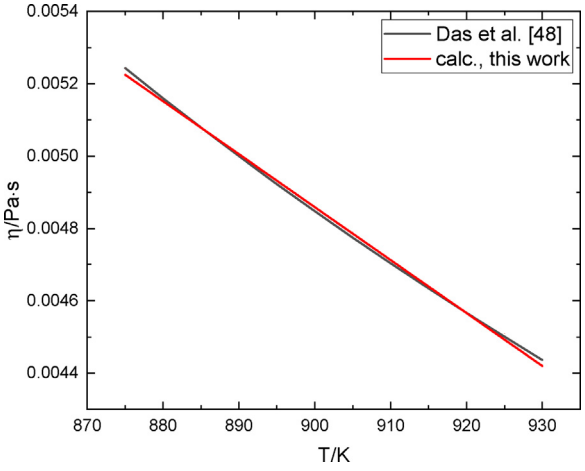

Fig. 12. Evolution of the viscosity with temperature, at composition $Li_{0.775}Th_{0.1995}U_{0.0255}F_{1.675}$, as reported by Das et al. [47], compared to the values computed in this work.

4. Conclusions

Building up from the descriptions of the pure end-members, the density and viscosity of three key binary systems for MSR technology have been modelled: LiF-ThF_4, LiF-UF_4, and NaCl-UCl_3. The density and viscosity of a composition belonging to the LiF-ThF_4-UF_4 ternary system, $Li_{0.775}Th_{0.1995}U_{0.0255}F_{1.675}$, have been modelled as well. All are linked to the corresponding thermodynamic assessments via the distribution of the quadruplet fractions, and the viscosities further depend on the densities. The agreement between the computed values and empirical fits (based on experimental data) is generally very good, although there is a clear need for more data, particularly in the ternary composition space, to further validate and re-parametrize the models as needed. The quasi-chemical model has become a widely used formalism in the description of molten salts, and the number of systems assessed is already substantial [86,87]. Thus, expanding databases of molten salt fuels beyond the thermodynamic properties, e.g. with density and viscosity parameters as herein, promises to be a powerful addition to the toolbox for MSR development.

Data availability

Thermodynamic database file available upon request.

Declaration of Competing Interest

The authors declare that they have no known competing financial interests or personal relationships that could have appeared to influence the work reported in this paper.

CRediT authorship contribution statement

J.A. Ocádiz Flores: Conceptualization, Methodology, Investigation, Formal analysis, Visualization, Data curation, Writing – original draft. **R.J.M. Konings:** Conceptualization, Supervision, Writing – review & editing. **A.L. Smith:** Conceptualization, Methodology, Supervision, Funding acquisition, Resources, Project administration, Writing – review & editing.

Acknowledgments

A.L. Smith acknowledges financial support from the Netherlands Organisation for Scientific Research (NWO) (project 722.016.005). J.A. Ocádiz Flores acknowledges the European Nuclear Education Network for supporting this work in the framework of the ENEN+ Project (mobility grant A-041841711), as well as CONACYT-SENER (grant 439146) for financial support. This work contributes to the European H2020 project SAMOSAFER funded by the European Commission (grant agreement no. 847527).

References

[1] J. Lane, H. MacPherson, F. Maslan, FLUID FUEL REACTORS: Molten Salt Reactors, Aqueous Homogeneous Reactors, Fluoride Reactors, Chloride Reactors, Liquid Metal Reactors and Why Liquid Fission, Addison-Wesley Pub. Co., 1958.
[2] R. Briant, A. Weinberg, Molten fluorides as power reactor fuels, Nuclear Science and Engineering 2 (6) (1957) 797–803.
[3] E. Bettis, R. Schroeder, G. Cristy, H. Savage, R. Affel, L. Hemphill, The aircraft reactor experiment-design and construction, Nuclear Science and Engineering 2 (6) (1957) 804–825.
[4] J. Bulmer, U.A.E. Commission, Fused Salt Fast Breeder: Reactor Design and Feasibility Study, CF (Series), United States Atomic Energy Commission, Technical Information Service Extension, 1957. https://books.google.nl/books?id=f0lOJb0x1jIC
[5] H. MacPherson, The molten salt reactor adventure, Nuclear Science and Engineering 90 (4) (1985) 374–380, doi:10.13182/NSE90-374.
[6] GIF, Annual report 2013, Generation IV International Forum, Tech. Rep., 2013. http://www.gen-4.org/gif/upload/docs/application/pdf/2014-06/gif_2013_annual_report-final.pdf
[7] T. Dolan, Molten salt reactors and thorium energy, Woodhead Publishing, 2017.
[8] M. Lin, M. Cheng, Z. Dai, Feasibility of an innovative long-life molten chloride–cooled reactor, Nuclear Science and Techniques 31 (4) (2020) 1–15.
[9] L. He, G. Li, S. Xia, J. Chen, Y. Zou, G. Liu, Effect of ^{37}Cl enrichment on neutrons in a molten chloride salt fast reactor, Nuclear Science and Techniques 31 (3) (2020) 1–12.
[10] M. Stika, Actinide Concentration Monitoring and Extraction from Molten Fluoride and Chloride Salts, The University of Utah, 2017 Ph.D. thesis.
[11] E. Merle. https://www.iaea.org/nptd-webinars/4-molten-salt-reactors-a-game-changer-in-the-Nuclear-industry.
[12] A. Pelton, S. Degterov, G. Eriksson, C. Robelin, Y. Dessureault, "The modified quasichemical model I—Binary solutions", Metallurgical and Materials Transactions B 31 (4) (2000) 651–659.
[13] C. Robelin, P. Chartrand, G. Eriksson, A density model for multicomponent liquids based on the modified quasichemical model: Application to the NaCl-Kcl-$MgCl_2$-$CaCl_2$ system, Metallurgical and Materials Transactions B 38 (6) (2007) 869–879.
[14] C. Robelin, P. Chartrand, A density model based on the modified quasichemical model and applied to the NaF-AlF_3-CaF_2-Al_2O_3 electrolyte, Metallurgical and Materials Transactions B 38 (6) (2007) 881–892.
[15] C. Robelin, P. Chartrand, A viscosity model for the (NaF + AlF_3 + CaF_2+ Al_2O_3) electrolyte, The Journal of Chemical Thermodynamics 43 (5) (2011) 764–774.
[16] J. Leitner, P. Voňka, D. Sedmidubský, P. Svoboda, Application of Neumann-Kopp rule for the estimation of heat capacity of mixed oxides, Thermochimica Acta 497 (1-2) (2010) 7–13, doi:10.1016/j.tca.2009.08.002. http://www.sciencedirect.com/science/article/pii/S0040603109003189
[17] A. Tosolin, E. Capelli, R. Konings, L. Luzzi, O. Beneš, Isobaric heat capacity of solid and liquid thorium tetrafluoride, Journal of Chemical & Engineering Data 64 (9) (2019) 3945–3950.
[18] E. Capelli, O. Beneš, M. Beilmann, R.J.M. Konings, "Thermodynamic investigation of the LiF-ThF_4 system ", The Journal of Chemical Thermodynamics 58 (2013) 110–116, doi:10.1016/j.jct.2012.10.013. http://www.sciencedirect.com/science/article/pii/S0021961412003990
[19] S. Mukherjee, S. Dash, Determination of gibbs energy of formation of $LiThF_5$, $LiTh_2F_9$, and $LiTh_4F_{17}$ in Li-Th-F system by using solid electrolyte galvanic cell, Journal of Solid State Electrochemistry 23 (11) (2019) 3043–3056.
[20] J. Ocádiz-Flores, A. Gheribi, J. Vlieland, K. Dardenne, J. Rothe, R. Konings, A. Smith, New insights and coupled modelling of the structural and thermodynamic properties of the LiF-UF_4 system, Journal of Molecular Liquids 331 (2021) 115820.
[21] V. Glushko, V. Gurvich L.V. Weitz, V. Medvedev, G. Hachkuruzov, V. Jungmann, G. Bergman, V. Baibuz, V. Yorish, The IVTAN data bank on the thermodynamic properties of individual substances, Nauka Publishing House, 1978.
[22] G. van Oudenaren, J. Ocadiz-Flores, A. Smith, Coupled structural-thermodynamic modelling of the molten salt system NaCl-UCl_3, Journal of Molecular Liquids (2021) 117470.
[23] W. Plato, Erstarrungserscheinungen an anorganischen salzen und salzgemischen. i, Zeitschrift für Physikalische Chemie 55 (1) (1906) 721–737.
[24] B. Pyashyenko, unknown, Metallurgiya 10 (11) (1935) 85.
[25] I. Murgulescu, et al., Heat capacities in molten alkaline halides, Rev. Roumaine Chim. 22 (5) (1977) 683–689.
[26] R. Dawson, E. Brackett, T. Brackett, A high temperature calorimeter; the enthalpies of α-aluminum oxide and sodium chloride, The Journal of Physical Chemistry 67 (8) (1963) 1669–1671.
[27] E. Capelli, R. Konings, Halides of the actinides and fission products relevant for molten salt reactors, Comprehensive Nuclear Materials, Elsevier, 2020.
[28] M. Chase, NIST-JANAF Thermochemical Tables (Journal of Physical and Chemical Reference Data Monograph No. 9), 1998.
[29] R. Konings, J. Van der Meer, E. Walle, Chemical aspects of molten salt reactor fuel, Technical Report, Tech. Rep., ITU-TN 2005/25, 2005.
[30] E. Capelli, O. Beneš, R. Konings, Thermodynamic assessment of the LiF-NaF-BeF_2-ThF_4-UF_4 system, Journal of Nuclear Materials 449 (1) (2014) 111–121, doi:10.1016/j.jnucmat.2014.03.009. http://www.sciencedirect.com/science/article/pii/S0022311514001184
[31] O. Beneš, M. Beilmann, R. Konings, Thermodynamic assessment of the LiF–NaF–ThF_4–UF_4 system, Journal of Nuclear Materials 405 (2) (2010) 186–198.
[32] J. Karlsruhe, JRCSMSD thermodynamic database on halide salts (not publicly available)., 2020.
[33] H. Matsuura, R. Takagi, L. Rycerz, M. Gaune-Escard, Enthalpies of mixing in molten UCl_3-NaCl system, Journal of Nuclear Science and Technology 39 (sup3) (2002) 632–634.
[34] A. Pelton, A general "geometric" thermodynamic model for multicomponent solutions, Calphad 25 (2) (2001) 319–328, doi:10.1016/S0364-5916(01)00052-9. http://www.sciencedirect.com/science/article/pii/S0364591601000529
[35] S. Glasstone, K.J. Laidler, H. Eyring, The theory of rate processes, McGraw-Hill, 1941.
[36] H. Eyring, D. Henderson, T. Ree, Thermodynamic and transport properties of liquids, in: Progress in International Research on Thermodynamic and Transport Properties, Elsevier, 1962, pp. 340–351.
[37] H. Eyring, Statistical mechanics and dynamics, Wiley, 1964.
[38] S. Mizani, Modeling the viscosity of liquid solutions used in aluminum alloys production, École Polytechnique de Montreal, 2008.
[39] R. Thoma, H. Insley, B. Landau, H. Friedman, W. Grimes, Phase equilibria in the fused salt systems LiF–ThF_4 and NaF–ThF_4, The Journal of Physical Chemistry 63 (8) (1959) 1266–1274.
[40] C. Barton, H. Friedman, W. Grimes, H. Insley, R. Moore, R. Thoma, Phase equilibria in the alkali fluoride-uranium tetrafluoride fused salt systems: I, the systems LiF-UF_4 and NaF-UF_4, Journal of the American Ceramic Society 41 (2) (1958) 63–69.
[41] Y. Jeongho, M. Smith, J. Tapp, A. Moller, H. zur Loye, Mild hydrothermal crystal growth, structure, and magnetic properties of ternary u (iv) containing fluorides: LiUF5, KU_2F_9, $K_7U_6F_{31}$, $RbUF_5$, RbU_2F_9, and RbU_3F_{13}, Inorganic Chemistry 53 (12) (2014) 6289–6298.
[42] O. Beneš, R. Konings, Thermodynamic evaluation of the NaCl–$MgCl_2$–UCl_3–$PuCl_3$ system, Journal of Nuclear Materials 375 (2) (2008) 202–208.
[43] E. Sooby, A. Nelson, J. White, P. McIntyre, Measurements of the liquidus surface and solidus transitions of the NaCl–UCl_3 and NaCl–UCl_3–$CeCl_3$ phase diagrams, Journal of Nuclear Materials 466 (2015) 280–285.
[44] C. Kraus, Phase Diagram of Some Complex Salts of Uranium with Halides of the Alkali and Alkaline Earth Metals, Technical Report, Office of Scientific and Technical Information, 1943. M-251
[45] C. Weaver, R. Thoma, H. Insley, H. Friedman, Phase equilibria in the systems UF_4-ThF_4 and LiF-UF_4-ThF_4, Journal of the American Ceramic Society 43 (4) (1960) 213–218.
[46] J. Van der Meer, R. Konings, H. Oonk, Thermodynamic assessment of the LiF–BeF_2–ThF_4–UF_4 system, Journal of Nuclear Materials 357 (1–3) (2006) 48–57.
[47] P. Das, S. Mukherjee, R. Mishra, S. Dash, Thermodynamic and physical properties of molten LiF-ThF_4-UF_4 salts mixture, Journal of Fluorine Chemistry 226 (2019) 109349, doi:10.1016/j.jfluchem.2019.109349. https://www.sciencedirect.com/science/article/pii/S0022113919301678
[48] G. Janz, F. Dampier, G. Lakshminarayanan, P. Lorenz, R. Tomkins, Molten salts: Volume 1. Electrical conductance, density, and viscosity data, U.S. Government Printing Office, 1968.

[49] B. Porter, R. Meaker, Density and molar volumes of binary fluoride mixtures, Report of investigations, US Department of the Interior, Bureau of Mines, 1966. 6836
[50] E. Brown, B. Porter, Electrical Conductivity and Density of Molten Systems of Uranium Tetrafluoride and Thorium Fluoride and Alkali Fluorides, Report of investigations, US Department of the Interior, Bureau of Mines, 1964. 6500
[51] I. Yaffe, E. van Artsdalen, Fused salts. Electrical conductance and density of fused halides. Chemistry Division Semiannual Progress Report, Oak Ridge National Laboratory, ORNL-2159, 1956.
[52] D. Hill, S. Cantor, W. Ward, Molar volumes in the LiF-ThF_4 system, Journal of Inorganic and Nuclear Chemistry 29 (1) (1967) 241–243.
[53] K. Taniuchi, T. Kanai, Densities of molten salts of some binary fluoride systems containing lithium fluoride, Science Reports of the Research Institutes Tohoku University Series A-Physics, Chemistry and Metallurgy 26 (6) (1977) 333–343.
[54] G. Janz, G. Gardner, U. Krebs, R. Tomkins, Molten salts: volume 4, part 1, fluorides and mixtures electrical conductance, density, viscosity, and surface tension data, Journal of Physical and Chemical Reference Data 3 (1) (1974) 1–115.
[55] M. Smirnov, V. Stepanov, Density and surface tension of molten alkali halides and their binary mixtures, Electrochimica Acta 27 (11) (1982) 1551–1563.
[56] A. Klimenkov, N. Kurbatov, S. Raspopin, Y. Chervinskii, Density and surface tension of molten mixtures of uranium tetrafluoride with lithium and sodium fluorides, Atomic Energy 56 (5) (1984) 339–341.
[57] S. Hara, K. Ogino, The densities and the surface tensions of fluoride melts, ISIJ International 29 (6) (1989) 477–485.
[58] V.Y. Chekhovskoi, A device for measuring the density and surface tension of melts, Instruments and Experimental Techniques 43 (3) (2000) 415–418.
[59] A. Kirshenbaum, J. Cahill, The density of molten thorium and uranium tetrafluorides, Journal of Inorganic and Nuclear chemistry 19 (1-2) (1961) 65–68.
[60] S. Cantor, D. Hill, W. Ward, Density of molten thf4: Increase of density on melting, Inorganic and Nuclear Chemistry Letters 2 (1) (1966) 15–18, doi:10.1016/0020-1650(66)80083-1. https://www.sciencedirect.com/science/article/pii/0020165066800831
[61] J. Van der Meer, R. Konings, Thermal and physical properties of molten fluorides for nuclear applications, Journal of Nuclear Materials 360 (1) (2007) 16–24.
[62] V. Desyatnik, S. Katyshev, S. Raspopin, Y.F. Chervinskii, Density, surface tension, and viscosity of uranium trichloride-sodium chloride melts, Soviet Atomic Energy 39 (1) (1975) 649–651.
[63] C. K. T. R. K. T. Mochinaga, J., Densities and equivalent conductivities of molten uranium trichloride and uranium trichloride-potassium chloride systems, J. Electrochem. Soc. Japan 37(9) (1969) 654–658.
[64] Y. Okamoto, P. Madden, K. Minato, X-ray diffraction and molecular dynamics simulation studies of molten uranium chloride, Journal of Nuclear Materials 344 (1-3) (2005) 109–114.
[65] B. Li, S. Dai, D. en Jiang, Molecular dynamics simulations of structural and transport properties of molten NaCl-UCl_3 using the polarizable-ion model, Journal of Molecular Liquids 299 (2020) 112184, doi:10.1016/j.molliq.2019.112184. https://www.sciencedirect.com/science/article/pii/S0167732219344629
[66] G. van Oudenaren, Advanced modelling of chloride salt systems for use in molten salt reactor fuels, Delft University of Technology, 2020.
[67] A. Baty, Molecular dynamics simulation of the transport properties of molten transuranic chloride salts, 2013.
[68] V. Desyatnik, A. Nechaev, Y. Chervinskii, Viscosities of molten mixtures of uranium tetrafluoride with alkali fluorides, Atomic Energy 46 (5) (1979) 408–409.
[69] Y. Chervinskii, V. Desyatnik, A. Nechaev, Molar viscosity of lithium and thorium fluoride melted mixtures, Zhurnal Fizicheskoi Khimii 56 (8) (1982) 1946–1949.
[70] V. Desyatnik, A. Nechaev, Y. Chervinskii, Viscosity of fused mixtures of beryllium fluoride with lithium and sodium fluorides, Journal of Applied Chemistry of the USSR 54 (10) (1981) 2035–2037.
[71] M. Smirnov, V. Stepanov, V. Khokhlov, A. Antonov, unknown, Zh. Fiz. Khim. 48 (11) (1974) 467.
[72] M. Vetyukov, G. Sipriya, unknown, J. Appl. Chem (USSR) 36 (1962) 1905.
[73] T. Ejima, Y. Sato, S. Yaegashi, T. Kijima, E. Takeuchi, K. Tamai, Viscosity of molten alkali fluorides, Nippon Kinzoku Gakkai-si 51 (4) (1987) 328–337.
[74] Y. Abe, O. Kosugiyama, A. Nagashima, Viscosity of lif-bef2 eutectic mixture (xbef2= 0.328) and lif single salt at elevated temperatures, Journal of Nuclear Materials 99 (2-3) (1981) 173–183.
[75] L. Dewan, Molecular dynamics simulation and topological analysis of the network structure of actinide-bearing Materials, Massachusetts Institute of Technology, 2013 Ph.D. thesis.
[76] I. Murgulescu, S. Zuca, Unknown, Zeitschrift für Physikalische Chemie 222 (300) (1963).
[77] L. J. K. J. R. J. E. M. B.C. Blanke, E.N. Bousquet, Density and viscosity of fused mixtures of lithium, beryllium, and uranium fluorides, Technical Report USAEC MLM-1086 (1956).
[78] K. Cho, T. Kuroda, J. Mochinaga, R. Takagi, Densities and equivalent conductivities of molten uranium trichloride-sodium chloride and uranium trichloride-(potassium chloride-sodium chloride eutectic) systems, J. Electrochem. Soc. Japan 37 (9) (1969) 658–661.
[79] V. Volkovich, I. May, C. Sharrad, H. Kinoshita, I. Polovov, A. Bhatt, J. Charnock, T. Griffiths, R. Lewin, Uranium speciation in molten salts from x-ray absorption and electronic absorption spectroscopy measurements, SpecialL Publication-Royal Society of Chemistry 305 (1) (2006) 485–490.
[80] C. Bessada, D. Zanghi, M. Salanne, A. Gil-Martin, M. Gibilaro, P. Chamelot, L. Massot, A. Nezu, H. Matsuura, Investigation of ionic local structure in molten salt fast reactor LiF-ThF_4-UF_4 fuel by exafs experiments and molecular dynamics simulations, Journal of Molecular Liquids 307 (2020) 112927, doi:10.1016/j.molliq.2020.112927. http://www.sciencedirect.com/science/article/pii/S0167732220304347
[81] A. Smith, M. Verleg, J. Vlieland, D.d. Haas, J. Ocádiz-Flores, P. Martin, J. Rothe, K. Dardenne, M. Salanne, A. Gheribi, et al., In situ high-temperature exafs measurements on radioactive and air-sensitive molten salt materials, Journal of Synchrotron Radiation 26 (1) (2019).
[82] L. Dewan, C. Simon, P. Madden, L. Hobbs, M. Salanne, Molecular dynamics simulation of the thermodynamic and transport properties of the molten salt fast reactor fuel LiF-ThF_4, Journal of Nuclear Materials 434 (1) (2013) 322–327, doi:10.1016/j.jnucmat.2012.12.006. Special Section on Spent Nuclear Fuel http://www.sciencedirect.com/science/article/pii/S0022311512006630
[83] R. Heaton, R. Brookes, P. Madden, M. Salanne, C. Simon, P. Turq, A first-principles description of liquid BeF_2 and its mixtures with LiF: 1. potential development and pure BeF_2, The Journal of Physical Chemistry B 110 (23) (2006) 11454–11460.
[84] M. Salanne, C. Simon, P. Turq, P. Madden, Conductivity- viscosity- structure: Unpicking the relationship in an ionic liquid, The Journal of Physical Chemistry B 111 (18) (2007) 4678–4684.
[85] J. Ocádiz-Flores, A. Gheribi, J. Vlieland, D. De Haas, K. Dardenne, J. Rothe, R. Konings, A. Smith, Examination of the short-range structure of molten salts: ThF_4, UF_4, and related alkali actinide fluoride systems, Physical Chemistry Chemical Physics 23 (18) (2021) 11091–11103.
[86] O. Beneš, Thermodynamics of molten salts for Nuclear applications, Ph.D. Dissertation, Institute of Chemical Technology, Prague, 2008 Ph.D. thesis.
[87] E. Capelli, Thermodynamic characterization of salt components for Molten Salt Reactor Fuel, Delft University of Technology, 2016 Ph.D. thesis.